ADVANCES IN ATMOSPHERIC SCIENCES, VOL. 40, MARCH 2023, 393–409

• **Original Paper** •

On the Influences of Urbanization on the Extreme Rainfall over Zhengzhou on 20 July 2021: A Convection-Permitting Ensemble Modeling Study※

Yali LUO*[1,2,3], Jiahua ZHANG[1,3], Miao YU*[1], Xudong LIANG[1], Rudi XIA[1], Yanyu GAO[1], Xiaoyu GAO[1], and Jinfang YIN[1]

[1]*State Key Laboratory of Severe Weather*, *Chinese Academy of Meteorological Sciences*, *Beijing* 100081, *China*

[2]*Collaborative Innovation Center on Forecast and Evaluation of Meteorological Disasters*, *Nanjing University of Information Science and Technology*, *Nanjing* 210044, *China*

[3]*School of Atmospheric Sciences*, *Chengdu University of Information Technology*, *Chengdu* 610225, *China*

(Received 12 March 2022; revised 8 May 2022; accepted 11 May 2022)

ABSTRACT

This study investigates the influences of urban land cover on the extreme rainfall event over the Zhengzhou city in central China on 20 July 2021 using the Weather Research and Forecasting model at a convection-permitting scale [1-km resolution in the innermost domain (d3)]. Two ensembles of simulation (CTRL, NURB), each consisting of 11 members with a multi-layer urban canopy model and various combinations of physics schemes, were conducted using different land cover scenarios: (i) the real urban land cover, (ii) all cities in d3 being replaced with natural land cover. The results suggest that CTRL reasonably reproduces the spatiotemporal evolution of rainstorms and the 24-h rainfall accumulation over the key region, although the maximum hourly rainfall is underestimated and displaced to the west or southwest by most members. The ensemble mean 24-h rainfall accumulation over the key region of heavy rainfall is reduced by 13%, and the maximum hourly rainfall simulated by each member is reduced by 15–70 mm in CTRL relative to NURB. The reduction in the simulated rainfall by urbanization is closely associated with numerous cities/towns to the south, southeast, and east of Zhengzhou. Their heating effects jointly lead to formation of anomalous upward motions in and above the planetary boundary layer (PBL), which exaggerates the PBL drying effect due to reduced evapotranspiration and also enhances the wind stilling effect due to increased surface friction in urban areas. As a result, the lateral inflows of moisture and high-θ_e (equivalent potential temperature) air from south and east to Zhengzhou are reduced.

Key words: urbanization, extreme rainfall, convection-permitting ensemble simulation, land–atmosphere interaction, boundary layer, water vapor transport

Citation: Luo, Y. L., J. H. Zhang, M. Yu, X. D. Liang, R. D. Xia, Y. Y. Gao, X. Y. Gao, and J. F. Yin, 2023: On the influences of urbanization on the extreme rainfall over Zhengzhou on 20 July 2021: A convection-permitting ensemble modeling study. *Adv. Atmos. Sci.*, **40**(3), 393−409, https://doi.org/10.1007/s00376-022-2048-8.

Article Highlights:

- The simulated 24-h rainfall accumulation and maximum hourly rainfall in Zhengzhou are reduced by 13% and 15–70 mm, respectively, by urbanization.
- The simulated rainfall reduction is closely associated with cities/towns to the south, southeast, and east of Zhengzhou.
- The warming, drying, and wind stilling effects of the upstream urban areas lead to reduction of lateral inflow of moisture to Zhengzhou.

1. Introduction

Urbanization could influence precipitation over and around cities through complex and sometimes compensating effects. Among them, the urban heat island (UHI)-induced thermal perturbation and its downstream advection are probably the first discovered and best known (Huff and Vogel,

※ This paper is a contribution to the special collection on the July 2021 Zhengzhou, Henan Extreme Rainfall Event.

* Corresponding authors: Yali LUO, Miao YU
Emails: ylluo@cma.gov.cn, yum@cma.gov.cn

1978; Hjelmfelt, 1982; Bornstein and Lin, 2000; Craig and Bornstein, 2002; Niyogi et al., 2011). More recently, two other urbanization influences on convection and precipitation have also been extensively discussed, namely, the building barrier effects of urban canyons (Bornstein and Lin, 2000; Guo et al., 2006; Zhang et al., 2009a; Miao et al., 2011) and the anthropogenic aerosol emissions as cloud condensation nuclei (CCN) sources (Rosenfeld, 2000; Jin and Shepherd, 2008; Bell et al., 2009; Ntelekos et al., 2009). Although it has been noted that urbanization impacts on local rainfall may differ from region to region, depending on geographical locations, nearby surface conditions, and regional climate regimes (Xiao et al., 2016; Fu et al., 2019; Zhang, 2020), long-term increases in rainfall are detected over rapid-urbanization regions and their downwind regions worldwide, e.g., America (Changnon, 1969; Changnon et al., 1981; Niyogi et al., 2011), China (Zhang et al., 2009b; Liang and Ding, 2017; Wai et al., 2017; Fu et al., 2019), India (Kishtawal et al., 2010), and Malaysia (Li et al., 2020). Positive trends in hourly rainfall extremes over the urban agglomerations in coastal China are partially attributed to the UHI effect based on the contrasting rainfall features in strong- versus weak-UHI pre-convective conditions, e.g., the rainfall extremes are mostly located over the urban cluster in strong-UHI condition while contrastingly situated near the coastline over South China in weak-UHI condition (Wu et al., 2019; Jiang et al., 2020).

In addition to climatological analysis, numerous case studies of urbanization effects on precipitation have been conducted during the past two decades, mostly through numerical modeling. Results show that urbanization can alter local low-level flow patterns, and the planetary boundary layer (PBL) structure and depth, through the UHI effect and urban canopy effect, facilitating convective initiation (CI) (Zhong and Yang, 2015; Zhong et al., 2015; Li et al., 2017, 2020; Yin et al., 2020; Sun et al., 2021). Moreover, the urban-induced rainfall enhancement may be modified by nearby complex terrain (Li et al., 2017; Yin et al., 2020) and land–water contrasts (Doan et al., 2021; Sun et al., 2021). Results also highlight the importance of flow regime analysis in understanding urban impacts on extreme rainfall (Yang et al., 2014, 2019). However, the understanding of urbanization influences on extremely heavy rainfall driven by strong synoptic and topographical forcing is limited due to few studies.

A historical rainfall event influenced Henan province in central China during 17–22 July 2021, characterized by a long duration, extreme rainfall accumulation, and a record-breaking hourly rain rate. This event took place under an anomalous large-scale circulation pattern, i.e., coexistence of a northward western North Pacific subtropical high (WNPSH) over Northeast Asia, Typhoon In-Fa (2021) over the East China Sea, and Typhoon Cempaka (2021) over the South China Sea (Yin et al., 2022). In particular, the strong low-level easterly airflow between the WNPSH and Typhoon In-Fa (2021) transported abundant moisture from the ocean to East China, which was further carried by the southeasterly airflow toward Henan province (Fig. 1) to support extreme rainfall. The mountains in western Henan (Mt. Songshan) and to its northwest and southwest (Mt. Taihang and Mt. Funiu; Fig. 2a), oriented roughly perpendicular to the approaching southeasterly winds, apparently played some role in the rainfall enhancement for this event (Wei et al., 2022). On 20 July 2021, devastating rainfall hit the capital city Zhengzhou (referred to as the **July 20 case** hereafter)

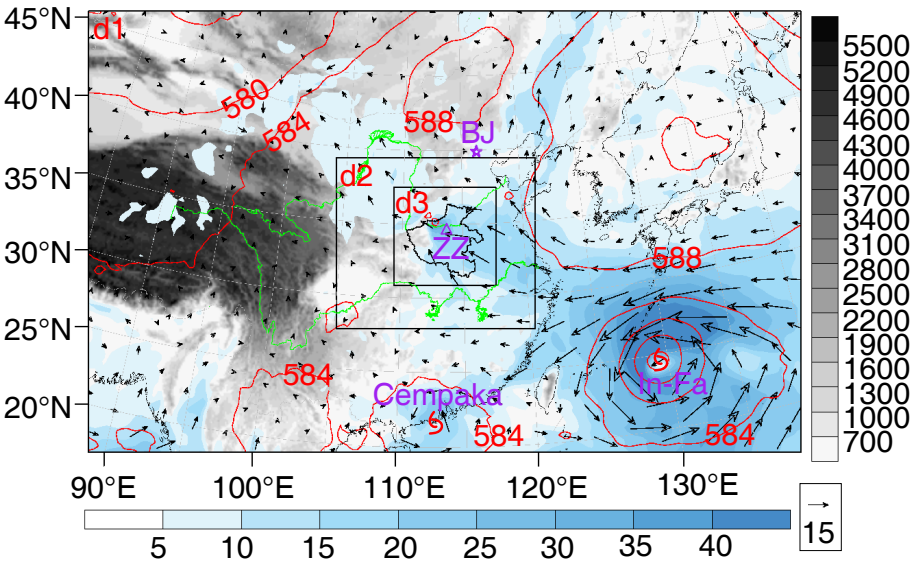

Fig. 1. Topography (gray shading, units: m; the same hereafter) in the simulation domains (d1–d3), overlaid by the water vapor flux at 925 hPa (arrow and blue shading; units: g cm^{-1} s^{-1} hPa^{-1}) and the 500-hPa geopotential height (red contours; units: dagpm; interval of 4 dagpm) at 1600 LST 20 July 2021. The black line in d3 outlines the boundary of Henan province. The Zhengzhou (ZZ) and Beijing (BJ) cities are labeled. Green lines denote the Yangtze River and Yellow River.

and caused severe flooding leading to more than 300 fatalities and tremendous economic losses. Note that the rainfall started to persistently influence Zhengzhou at about 0000 local standard time (LST; LST = UTC + 8) 18 July 2021, which is two days prior to the occurrence of heavy rainfall on 20 July 2021 (not shown).

In addition to Zhengzhou city, there are many other cities and towns in central and eastern China (Fig. 2b), a result of the rapid urbanization in China since mid-1990s. How do the Zhengzhou city itself, and the extensively distributed, upstream urban areas influence the heavy rainfall on 20 July 2021? To what extent, and through what mechanisms? In this study, we make efforts to answer these questions through numerical modeling. Specifically, two ensemble experiments, each consisting of 11 members with the highest horizontal grid spacing of 1 km, are conducted. The layout of the paper is as follows: model setup and verification will be described in section 2; analysis of urbanization impacts on the simulated rainfall and relevant processes will be presented in section 3; summary and conclusions will be given in section 4.

2. Design and verification of CTRL

2.1. *Description of CTRL*

To isolate the urbanization effects on the **July 20 case**, we utilize a one-way triply-nested (9/3/1 km; the three domains are shown in Fig. 1) version of the Weather Research and Forecasting (WRF) Model (version V4.0.3; Skamarock et al., 2008) to conduct simulations. The innermost domain (d3) is centered at Zhengzhou city and covers Henan province and its adjacent areas. The outermost domain (d1) covers the major large-scale weather systems, namely, the WNPSH over Northeast Asia, Typhoon In-Fa (2021) over the East China Sea, and Typhoon Cempaka (2021) over the South China Sea. There are 57 vertical layers with 8–9 layers in the lowest 1 km above the ground (see Table 1 for summary of the simulation design). All the

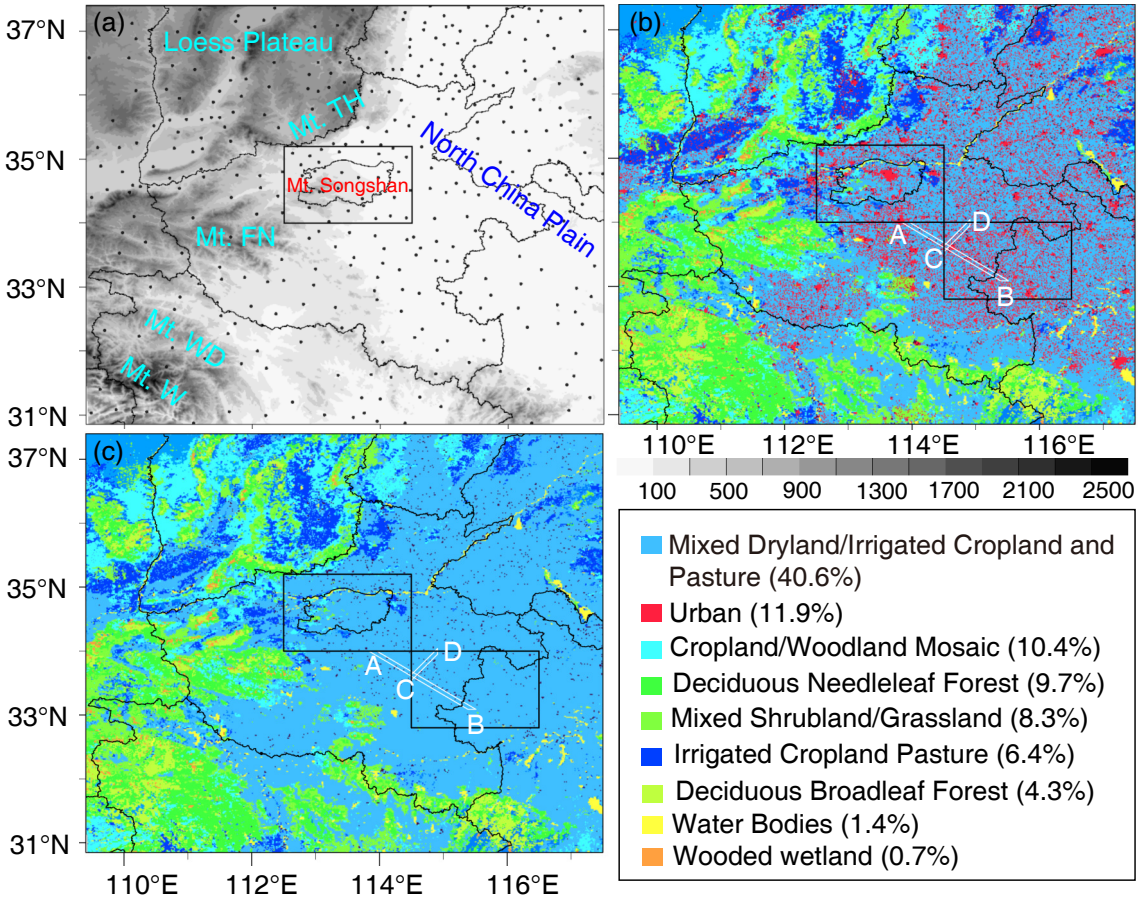

Fig. 2. (a) Topography (units: m) in the innermost domain (d3) of the simulations. Dots denote the national-level surface weather stations. The Loess Plateau, Mt. Songshan, Mt. Taihang (TH), Mt. Funiu (FN), Mt. Wudang (WD), Mt. Wu (W), and North China Plain are labeled. Land-use/land type map used in the (b) CTRL and (c) NURB experiments, respectively. The boundary of Zhengzhou city is outlined and embedded in a rectangle box, which denotes the key region of this study (approximately 34.0°–35.2°N, 112.5°–114.5°E). The other rectangle to the southeast is used to plot the red lines in Fig. 10. Lines CD and AB represent the locations of cross sections used in Figs. 11 and 12, respectively. Names and areal fractions (%) of the land cover/land-use types within d3 in CTRL are labeled at the lower right.

domains are initialized at 2000 LST on 19 July and integrated for 28 h, as this study focuses on the heavy rainfall on 20 July 2021. Numerical experiments initialized earlier (e.g., at 0800 LST) are also conducted, but they produce larger rainfall biases and thus are not used in this article. The ERA5 reanalysis data (ECMWF, 2017) is used to generate the initial state and lateral boundary conditions at an interval of 6 h.

The detailed evolution of the rainstorms and the spatiotemporal distributions of rainfall in the July 20 case show notable differences between the WRF model simulations and the observations, which is associated with uncertainties in the model initial state and lateral boundary conditions, as well as the physics parameterizations. To at least partially account for those uncertainties and increase the robustness of the simulation results, the control experiment (CTRL), consisting of 11 members, is conducted using various combinations of six cloud microphysics schemes and two PBL schemes (Table 2), i.e., the Thompson (Thompson et al., 2008), Thompson aerosol-aware (Thompson and Eidhammer, 2014), WDM6 (Lim and Hong, 2010), Morrison (Morrison et al., 2009), Morrison with CESM aerosol, and P3 (Morrison and Milbrandt, 2015) microphysics schemes, and the MYJ (Janjić, 1990, 2002) and Boulac (Bougeault and Lacarrere, 1989) PBL schemes. Other physics schemes (such as cumulus convection, longwave and shortwave radiation, urban physics, and land surface) utilized in the experiment are the same among all the members (Table 1). The Kain–Fritsch convective parameterization scheme (Kain, 2004) is used in d1, and convective parameterization is turned off in d2 and d3. The multilayer urban canopy model (BEP; Martilli, 2002) is coupled with the PBL scheme to represent exchanges of sensible heat, latent heat, and momentum between the PBL and urban surfaces in the simulations. The Noah land surface model (LSM; Chen and Dudhia, 2001; Ek et al., 2003) is used.

The CTRL experiment uses the Year 2015 land use/land type (as shown in Fig. 2b) derived from the 30-m resolution land-use data from the Resources and Environment Scientific Data Center, Chinese Academy of Sciences (http://www.resdc.cn/data.aspx?DATAID598). This data includes six land-use types (croplands, forest, grasslands, water bodies, built-up lands, and others) and is used to generate the USGS 24-category land use/land type of 1-km resolution, including the low-, medium-, and high-density residential urban classes with fractions of the built-up area of 0.5–0.9, 0.9–0.95, and 0.95–1, respectively. The land surface in d3 is covered by urban (11.9%) and a variety of land/vegetation types, such as the mixed dryland/irrigated cropland and pasture (40.6%), cropland/woodland mosaic (10.4%), deciduous needleleaf forest (9.7%), mixed shrubland/grassland (8.3%), and irrigated cropland pasture (6.4%).

2.2. *Model verification*

The model verification is conducted for d3, which has

Table 1. Summary of the simulation design.

	Simulation design		
Model (Version)	WRF (V4.0.3)		
Domains	d1	d2	d3
Grid points (x, y)	(601, 372)	(502, 433)	(775, 742)
Grid spacing (km)	9	3	1
Vertical layers	57		
Sigma values	1, 0.9938147, 0.9859506, 0.9760143, 0.9635575, 0.9480931, 0.9291238, 0.9061912, 0.8789424, 0.847208, 0.8110777, 0.770949, 0.7275254, 0.682155, 0.6394231, 0.5991763, 0.5612702, 0.5255684, 0.4919429, 0.4602729, 0.4304447, 0.4023511, 0.3758914, 0.3509704, 0.3274987, 0.3053921, 0.284571, 0.2649608, 0.246491, 0.2290954, 0.2127114, 0.1972803, 0.1827465, 0.1690579, 0.1561655, 0.1440227, 0.1325862, 0.1218148, 0.1116698, 0.1021147, 0.09311533, 0.08463936, 0.0766563, 0.0691375, 0.06205596, 0.05538623, 0.04910441, 0.0431879, 0.03761547, 0.03236707, 0.02742394, 0.02276827, 0.01838336, 0.01425343, 0.0103637, 0.00670018, 0.003249712, 0		
Cumulus convection	Kain-Fritsch (Kain 2004)	off	off
Longwave radiation	RRTM (Mlawer et al., 1997)		
Shortwave radiation	Dudhia (Dudhia, 1989)		
Urban physics	Multi-layer urban canopy model (BEP; Martilli, 2002)		
Land surface	Noah land surface model (Chen and Dudhia, 2001; Ek et al., 2003)		
Microphysics	See Table 2		
PBL physics	See Table 2		

Table 2. Cloud/precipitation microphysics schemes and PBL schemes used in the ensemble modeling. The number 28 and 40 denote the Thompson aerosol-aware scheme and Morrison double-moment scheme with CESM aerosol, respectively.

	Mem1	Mem2	Mem3	Mem4	Mem5	Mem6	Mem7	Mem8	Mem9	Mem10	Mem11
Microphysics	28	28	40	40	Thompson	Thompson	Morrison	Morrison	WDM6	WDM6	P3
PBL	MYJ	Boulac	MYJ	Boulac	MYJ	Boulac	MYJ	Boulac	MYJ	Boulac	MYJ

the highest horizontal resolution of 1 km and can better capture the evolution of extreme rainfall-producing storms compared to d1 and d2, which have coarser resolutions. The simulated rainfall from the ensemble mean and each member of CTRL are compared carefully with the gauge observations in this subsection. The analysis period of the simulation results is 24 h from 0000 LST 20 July to 0000 LST 21 July 2021 (excluding the first 4-h spin-up period).

2.2.1. *Spatial distribution of 24-h rainfall accumulation*

Firstly, the spatial distribution of the 24-h rainfall accumulation is examined (Fig. 3). The heavy rainfall (> 200 mm) in the observations is mostly distributed over Zhengzhou city, as well as the eastern side of Mt. Funiu to the city's southwest and the low lands to the city's northeast (i.e., the key region of this study defined by a rectangle in Fig. 3a). The individual simulations generally reproduce the

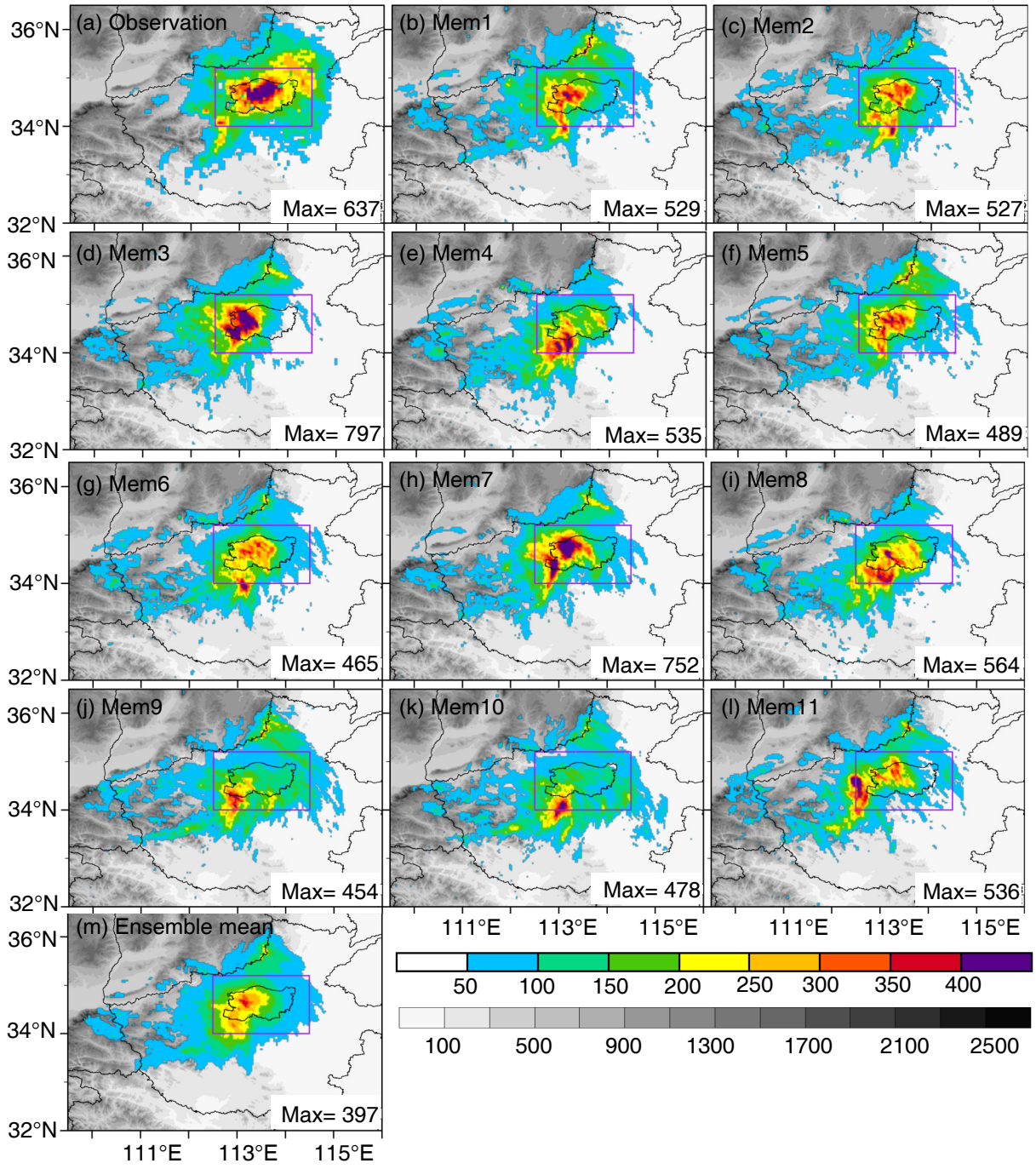

Fig. 3. Distribution of rainfall accumulation (units: mm; color shadings) during 0000 LST 20 July to 0000 LST 21 July 2021 in the (a) gauge observations, (b–l) Member 1 to Member 11 of CTRL, and (m) ensemble mean of CTRL. Purple boxes denote the key region of this study. The boundaries of Zhengzhou city and relevant provinces are outlined. Gray shadings denote terrain height (units: m).

heavy rainfall over Zhengzhou and its southwest, while they underestimate the rainfall to the northeast of Zhengzhou (Figs. 3b–l). A few members produce a major rainfall center to the southwest of the key region, rather than inside it (Figs. 3e, j, k). The maximum rainfall accumulation (639.8 mm) is underestimated by most (9 out of 11; 82%) members, but it is overestimated by members 3 and 7 (797.2 mm, 752.0 mm), which use the MYJ PBL scheme with the Morrison microphysics scheme or the Morrison scheme with CESM aerosol, respectively. The maximum rainfall accumulation is displaced to the west or southwest (i.e., at the foot of Mt. Songshan) in the simulations, which can be seen more clearly in Fig. 4a. The ensemble-mean heavy rainfall is mostly distributed over the key region, with a reduced amount compared with the observations (cf. Figs. 3m and 3a).

A Taylor diagram can concisely summarize the degree of correspondence between simulated and observed fields or time series (Taylor, 2001). It is used here to summarize the performance of WRF in simulating the 24-h rainfall accumulation over d3 (Fig. 4b). The gauge observation is used as the reference field, which is located at the point where the correlation is 1.0 and the normalized standard deviation is 1.0 in Fig. 4b. The correlation coefficients of the CTRL simulations are about 0.65–0.75, confirming that the CTRL simulations reasonably reproduce the overall distribution of the 24-h rainfall accumulation. The normalized standard deviations are mostly 0.6–0.8, mainly due to the underestimation of horizontal span and/or amount of the heavy rainfall by the simulations. Moreover, the d3-averaged rainfall accumulation is underestimated by 5%–10% in eight members and <5% in three members.

2.2.2. *Spatiotemporal evolution of intense short-term rainfall*

Intense short-term rainfall (> 20 mm h^{-1}) is mainly produced in the western portion of Zhengzhou (i.e., over Mt. Songshan) and to its southwest along the east side of Mt. Funiu during 0000–0300 LST in the observations (Fig. 5a), suggesting its close association with terrain. Later on, the intense rainfall in Zhengzhou extends slightly eastward during 0300–0600 LST (Fig. 5b) and is produced again in west Zhengzhou during 0600–0900 LST (Fig. 5c), while the intense rainfall to the southwest moves toward the key region (Figs. 5b, c). During 0900–1200 LST, intense rainfall is mostly located over the key region, especially its western portion, with another northwest–southeast oriented band of intense rainfall to its northeast (Fig. 5d). In the early afternoon, intense rainfall is continuously produced over western Zhengzhou and extends eastward to central and eastern Zhengzhou after about 1400 LST (Figs. 5e). Historical hourly rainfall of 201.9 mm is observed in central downtown Zhengzhou at 1700 LST, when the area of intense short-term rainfall shrinks. The increased rainfall extremity and the more localized extreme rainfall likely result from the merging of convective cells and formation of an arc-shaped surface convergence zone which favors the development of convective updrafts in a three-quarter circle around the storm (Yin et al., 2022).

To compare with the observations, occurrence frequency

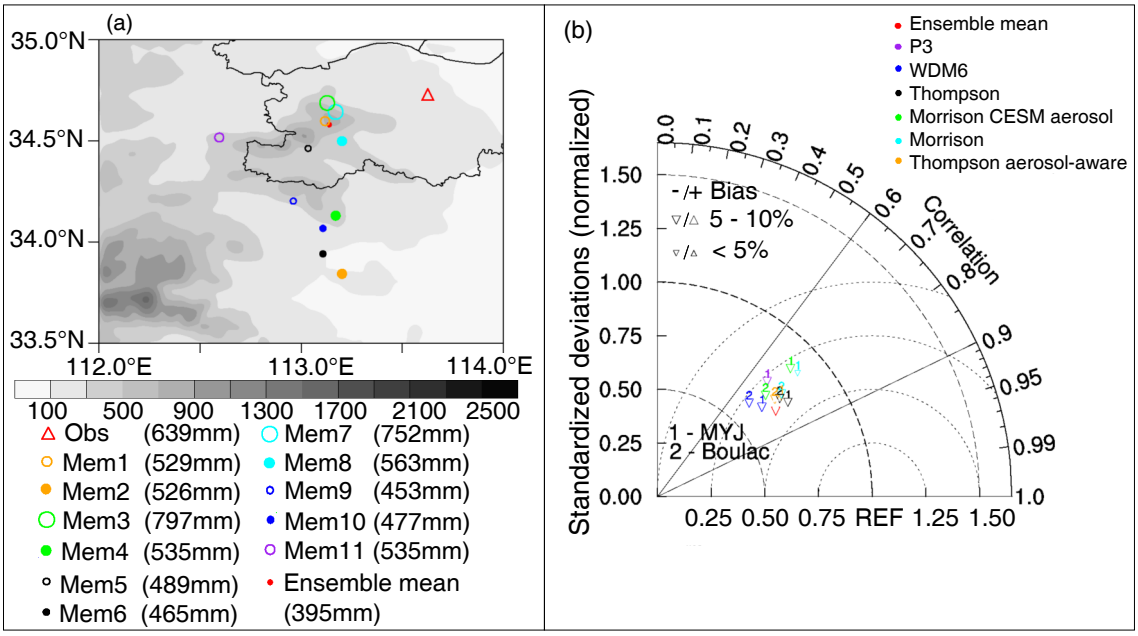

Fig. 4. (a) Location and amount of the maximum 24-h (ending at 0000 LST 21 July 2021) rainfall accumulation (units: mm) from the gauge observations, Member 1 to Member 11 of CTRL, and ensemble mean of CTRL. Gray shadings denote terrain height (units: m). (b) Taylor diagram for the 24-h rainfall accumulation over d3. The reference field is the AWS observation. Triangles denote the 24-h rainfall accumulation from the 11 members of CTRL and their ensemble mean, with the downward triangle indicating a negative bias in the rainfall accumulation averaged over all the AWSs.

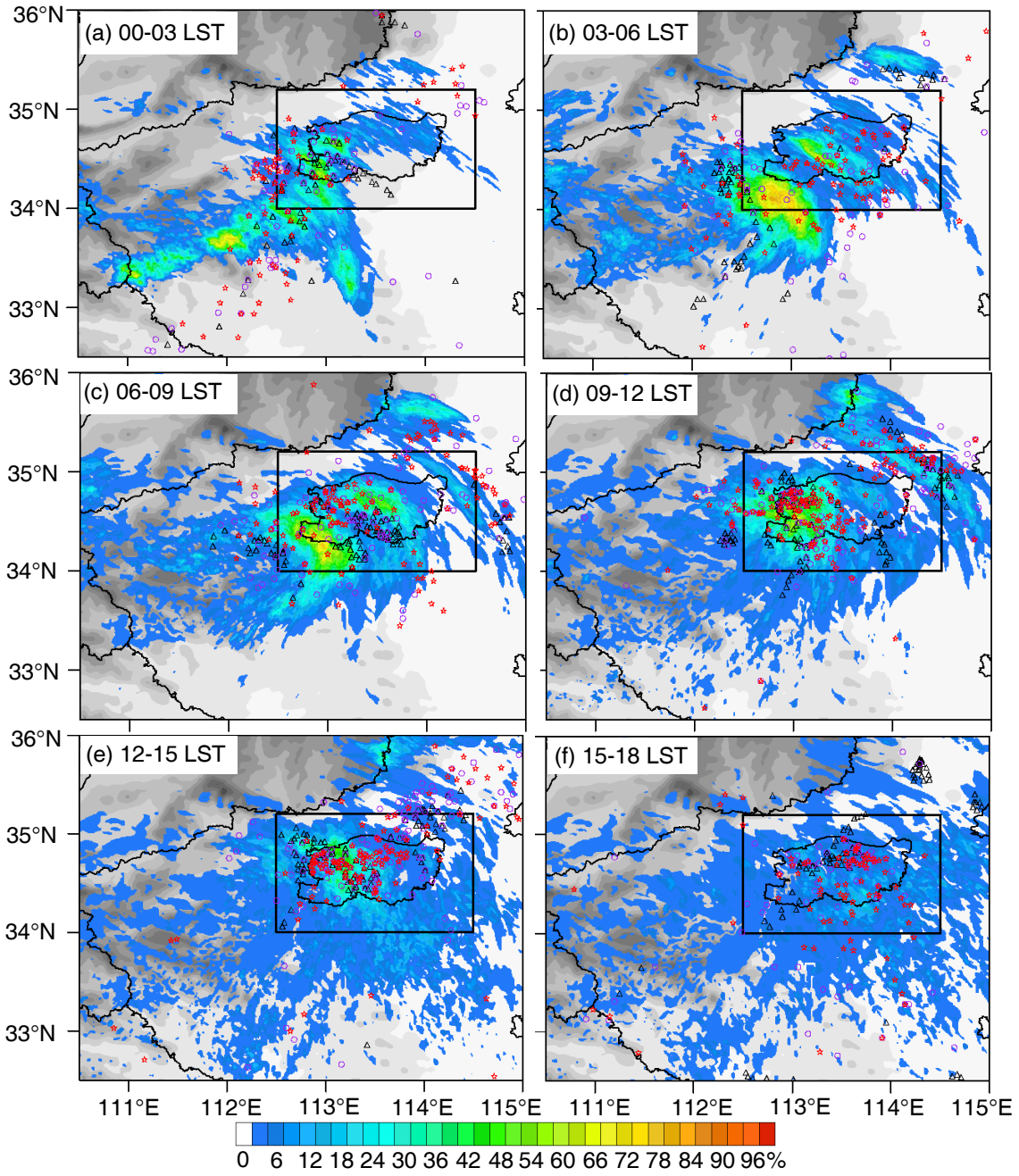

Fig. 5. Occurrence frequency (%) of intense short-term rainfall (≥20 mm h^{-1}) in the 11 members of CTRL during each 3-h period (color shadings) overlaid by the intense short-term rainfall observed at the AWSs (black triangle, purple circle, and red star denoting those during the 1st, 2nd, and 3rd hour, respectively). Gray shadings represent terrain heights (units: m; the same as in Fig. 4a).

(%) of intense short-term rainfall in CTRL is calculated at each grid point in d3 for each 3-h subperiod. The results are shown as shadings in Fig. 5. Clearly, the CTRL simulations reproduce the major features of intense rainfall as observed, e.g., its northeastward movement from Mt. Funiu during the nocturnal hours, its concentration over the western key region in the morning and early afternoon, and its occurrence to the northeast during 0900 to 1500 LST. However, the simulations tend to underestimate the occurrence of intense rainfall during 1500–1800 LST (Fig. 5f). The maximum hourly rainfall over the key region is produced earlier in the simulations, with a smaller amount (70–117 mm) than the observations, and is displaced mostly to the west or southwest at Mt. Songshan (Fig. 6a). These timing and position biases are common in real-data simulations (e.g., Davis and Galarneau, 2009; Xu et al., 2015; Abulikemu et al., 2019). Despite these biases, the simulations mostly generate a localized rainstorm over Zhengzhou in the early to mid-afternoon, which is at least qualitatively similar to the observations (cf. Figs. 6b, c).

The above results collectively suggest that the CTRL simulations reasonably capture not only the production of extreme rainfall accumulation over the key region, but also the overall evolution of intense short-term rainfall, although the maximum hourly rainfall is underestimated and displaced to the west or southwest. Therefore, with this limitation in mind, we conduct a sensitivity experiment to investigate the urbanization impacts on the rainfall in the July 20 case.

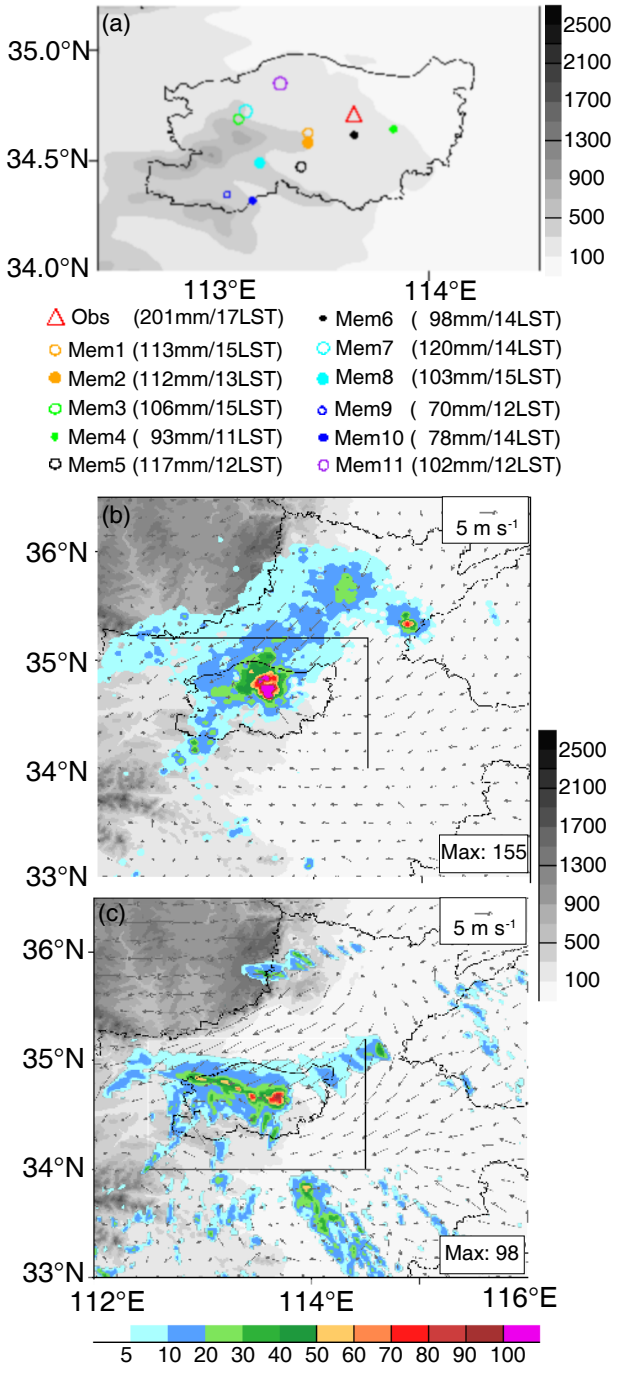

Fig. 6. (a) Spatial distribution of maximal hourly rainfall over Zhengzhou from the observation and the 11 simulations (Member 1 to Member 11) of CTRL. The time and rainfall amount are labeled at the bottom. (b) Hourly rainfall distribution (units: mm) in the observation during 1500–1600 LST 20 July 2021 overlaid with 10-m winds at 1600 LST. (c) The same as (b), except for in Member 6 of CTRL during 1300–1400 LST 20 July 2021 overlaid with 10-m winds at 1400 LST. Gray shadings denote terrain heights (units: m).

3. Analysis of urbanization influences

The sensitivity experiment (NURB) is identical to CTRL except that the urban areas in d3 are replaced with the most common land type nearby, i.e., the mixed dryland/irrigated cropland and pasture (Fig. 2c). The differences in the results between CTRL and NURB (CTRL minus NURB) are used in this section to discuss the urbanization impacts. The analysis period in this section is the same as that used in subsection 2.2 for the model verification, i.e., from 0000 LST 20 July to 0000 LST 21 July 2021, as this study aims at exploring possible urbanization influences on the heavy rainfall over Zhengzhou on 20 July 2021.

3.1. *Impacts on rainfall*

The ensemble-mean 24-h rainfall accumulation is generally decreased over the key region in CTRL relative to NURB, with the maximum reduction of rainfall being up to 163.3 mm in western Zhengzhou (Fig. 7a). The key region-averaged 24-h rainfall accumulation is reduced by 17.4 mm (13%) relative to NURB. To examine the temporal variation of the urbanization-induced difference in the key region-averaged hourly rainfall, the difference between each pair of members is divided by the corresponding rainfall amount in NURB to measure the relative difference. Consistent with Fig. 7a, urbanization leads to a reduction of about 5% in the ensemble mean during the earlier nocturnal hours, 10% in the late morning, 20% in the early afternoon, and 30% in the late evening hours (Fig. 7b). The standard deviations increase (longer bars in Fig. 7b) after 1100 LST, reflecting the growing spread among the members. Moreover, the maximum hourly rainfall in the key region is also decreased by 15 to 70 mm with the presence of cities. The production of maximum hourly rainfall in the key region is delayed by 1–3 h in five members and by 6 h in one member, at the same time as NURB in two members, and advanced by 1 h or 3 h in the other two members (Fig. 7c).

These results indicate that urbanization leads to non-negligible rainfall reduction over the key region, in both areal average amount and grid-point maximum value. In the following subsection, we will analyze the physical processes of relevance to the simulated rainfall reduction by urbanization.

3.2. *Influences on relevant physical processes*

The surface sensible heat flux (SHF) and latent heat flux (LHF) are small over the key region during the analysis period. The region-averaged SHF and LHF in the ensemble mean of CTRL increase rapidly after about 0700 LST and reach their maximum values of about 35 W m^{-2} and 90 W m^{-2}, respectively, at 1300–1400 LST (Fig. 8). In comparison, the SHF and LHF over the surrounding areas to the south, southeast, and east are much larger, e.g., mostly

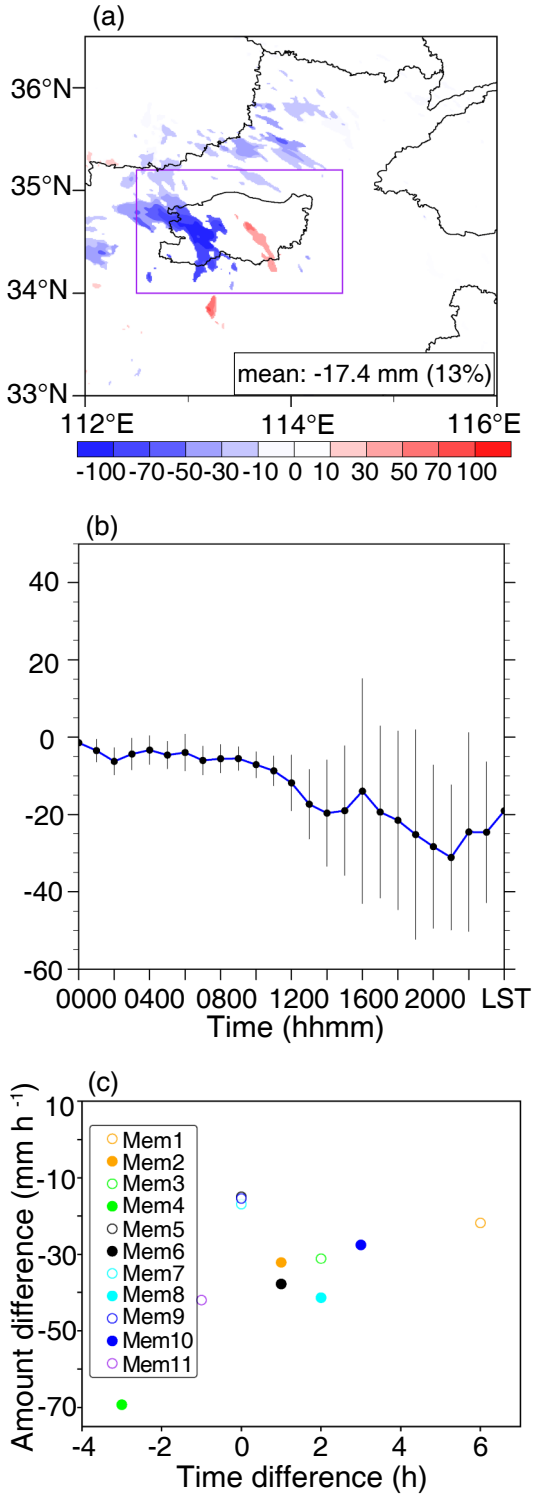

Fig. 7. (a) Spatial distribution of differences (CTRL minus NURB) in the ensemble-mean 24-h rainfall accumulation (units: mm). Only the differences that pass the Student's *t* test (confidence level of 95%) are shown. The purple box outlines the key region of this study. (b) Time series of relative difference (%) of hourly rainfall accumulation averaged over the key region: the ensemble mean (solid line with dots) plus/minus the standard deviation among the members (gray bar). (c) Difference between each pair of members in the amount and time of maximum hourly precipitation over the key region.

beyond 100 W m^{-2} (SHF) and 250 W m^{-2} (LHF) at 1400 LST, respectively (Figs. 9a, b). These regional variations are apparently due to the persistent rainfall over the key region. As a result, the PBL over the key region in CTRL hardly grows during the daytime (black solid lines in Fig. 10), in contrast to the development of a well-mixed boundary layer to its southeast (red solid lines in Fig. 10). The height of a well-mixed PBL can be estimated as where the vertical gradient of potential temperature is the maximum. The PBL top remains below about 300 m in the key region until 1600 LST but increases to about 1.1–1.2 km to its southeast (Fig. 10f). The small surface fluxes and lack of an evident UHI effect suggest that the local urbanization in Zhengzhou possibly has a limited impact on the rainfall for the July 20 case.

The small surface fluxes over the key region are also obvious in the NURB experiment (dashed lines in Fig. 8; Figs. 9c, d; black dashed lines in Fig. 10). Compared to CTRL, surface SHF and LHF averaged over the key region in NURB are slightly reduced and increased, respectively, throughout the day (Fig. 8; Figs. 9e, f), which is consistent with the well-known urban-induced influences on land–atmosphere interactions. The 24-h averaged differences between CTRL and NURB are 3.7 W m^{-2} (SHF) and –8.9 W m^{-2} (LHF). Equivalent potential temperature (θ_e) in the PBL is lower in CTRL than NURB, with smaller magnitudes of reduction than those to the southeast (Figs. 10a–c) where numerous cities/towns are scattered over the plain (Fig. 2b). The urbanization-induced lower θ_e over the key region is mainly caused by a reduction of moisture (black lines in Figs. 10g–i), as the potential temperature changes little (black lines in Figs. 10d, e, f). The θ_e reduction could lead to weakened convective intensity and the decreased rainfall amount over the key region, as higher PBL θ_e is generally more favorable for rainstorm development.

The urbanization-induced reductions of θ_e and moisture in the PBL over the key region could be contributed by the decrease of LHF from the local ground surface. However, this is unlikely to be the major contributor given the small magnitude of the LHF reduction (–8.9 W m^{-2}). As the low-level southeasterly airflow (Fig. 1) plays an important role in the July 20 case (Yin et al., 2022), and obvious UHI and urban drying effects are present over the southeast region (red lines in Figs. 10g–i), we further analyze whether the upstream cities/towns influence the transportation of high-θ_e air into the key region. The horizontal flux of θ_e across line CD (located near the southeast corner of the key region; Figs. 2b, c) toward the key region is shown in Fig. 11. The horizontal flux increases with height in the PBL due to the increase of horizontal wind speed with height. A decrease of the θ_e flux is found in CTRL with the presence of cities/towns relative to NURB.

To better understand this, vertical cross sections along the southeast–northwest oriented AB line (perpendicular to CD; Figs. 2b, c) are examined. The southeasterly airflow passing over the warmer and drier surface from the southeast to

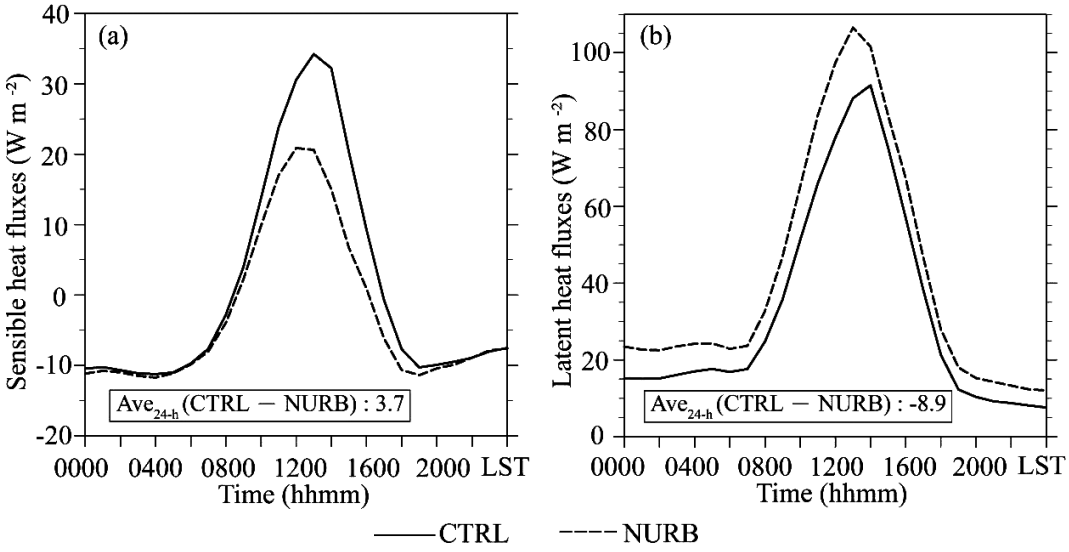

Fig. 8. Time series of (a) surface sensible heat flux and (b) latent heat flux (W m^{-2}) averaged over the key region for the ensemble mean of CTRL (solid line) and NURB (dashed line), respectively. The differences of the 24-h averaged values from CTRL and NURB (CTRL minus NURB) are labeled.

approach the key region can be clearly seen in Fig. 12a. The PBL top at 1300 LST is located at about 1.0 km at the southeast end of the cross section and decreases gradually to about 0.7 km at the northwest end due to the rain-related evaporative cooling in the morning (Figs. 5c, d). Consistently, the urban heating and drying effects in the PBL are more prominent to the southeast, where the near-surface temperature increases more than 1°C and specific humidity decreases up to 2.2 g kg^{-1} in CTRL relative to NURB. Such urban influences exist over the extensive contiguous area due to the "radiation" of the UHI effects being stronger to the southeast. The UHI effects of numerous cities/towns jointly lead to the formation of anomalous upward motion to the southeast and the formation of compensating subsidence near the key region, where the associated adiabatic heating leads to positive temperature differences. The anomalous upward motion is not due to different locations of the convective cells, as the simulated rainfall is mostly distributed over the key region and its north, west, and southwest (Fig. 3). The upward motion to the southeast leads to adiabatic cooling above the PBL and transports moisture to the upper levels, which exacerbates the PBL drying caused by reduced evapotranspiration in urban areas (Matheson and Ashie, 2008). The wind-vector differences in the PBL point toward the southeast, indicating weakening of the southeasterly winds toward Zhengzhou. This wind speed reduction is contributed directly by the higher roughness elements in urban areas, i.e., the wind stilling effect due to increased surface friction (Wang et al., 2009), and indirectly by the abovementioned UHI-induced circulation changes with the PBL air tending to flow away from the key region.

The reduced wind speed and moisture content in the PBL over the upstream areas together result in decreased moisture transport into the key region (Fig. 13). The key region obtains moisture from the south and east and losses it to the west and north, which is mainly determined by the large-scale circulation (Fig. 1). Despite the different temporal evolutions of the moisture inflows across the east and south boundaries, the urban-induced reduction is clearly seen throughout the day across the east and south boundaries (Figs. 13b, d), as well as in the net inflow of moisture (Fig. 13e). The 24-h averaged changes in the moisture flux vertically integrated from the surface to 800 hPa are the largest across the south boundary (-46.7×10^5 kg s^{-1}), followed by the east boundary (-23.7×10^5 kg s^{-1}). The outflow of moisture across the north and west boundaries decreases by 10.2×10^5 kg s^{-1} and 15.7×10^5 kg s^{-1}, respectively. The reduction of net inflow of moisture is -46.7×10^5 kg s^{-1}. Associated with the reduced lateral inflows of moisture (Fig. 13) and higher θ_e (Fig. 11) to the key region, the area of convective updrafts over the key region is reduced in CTRL relative to NURB, as suggested by the decreased number of grid points with air vertical velocity (w) > 2 m s^{-1} (Fig. 14) throughout the troposphere. The smaller area of convective updrafts could contribute to the decreased rainfall amount over the key region.

4. Summary and conclusions

The understanding of urbanization impacts on extremely heavy rainfall driven by strong synoptic and topographical forcing is limited due to few studies. This study investigates possible influences of urbanization on the heavy rainfall over Zhengzhou on 20 July 2021 through numerical modeling using the WRF model. To increase the robustness of the modeling results, two ensembles (each consisting of 11 members) are conducted using different land cover scenarios. One includes the cities (CTRL), and the other replaces the cities with the most common land type nearby, i.e., the mixed dryland/irrigated cropland and pasture

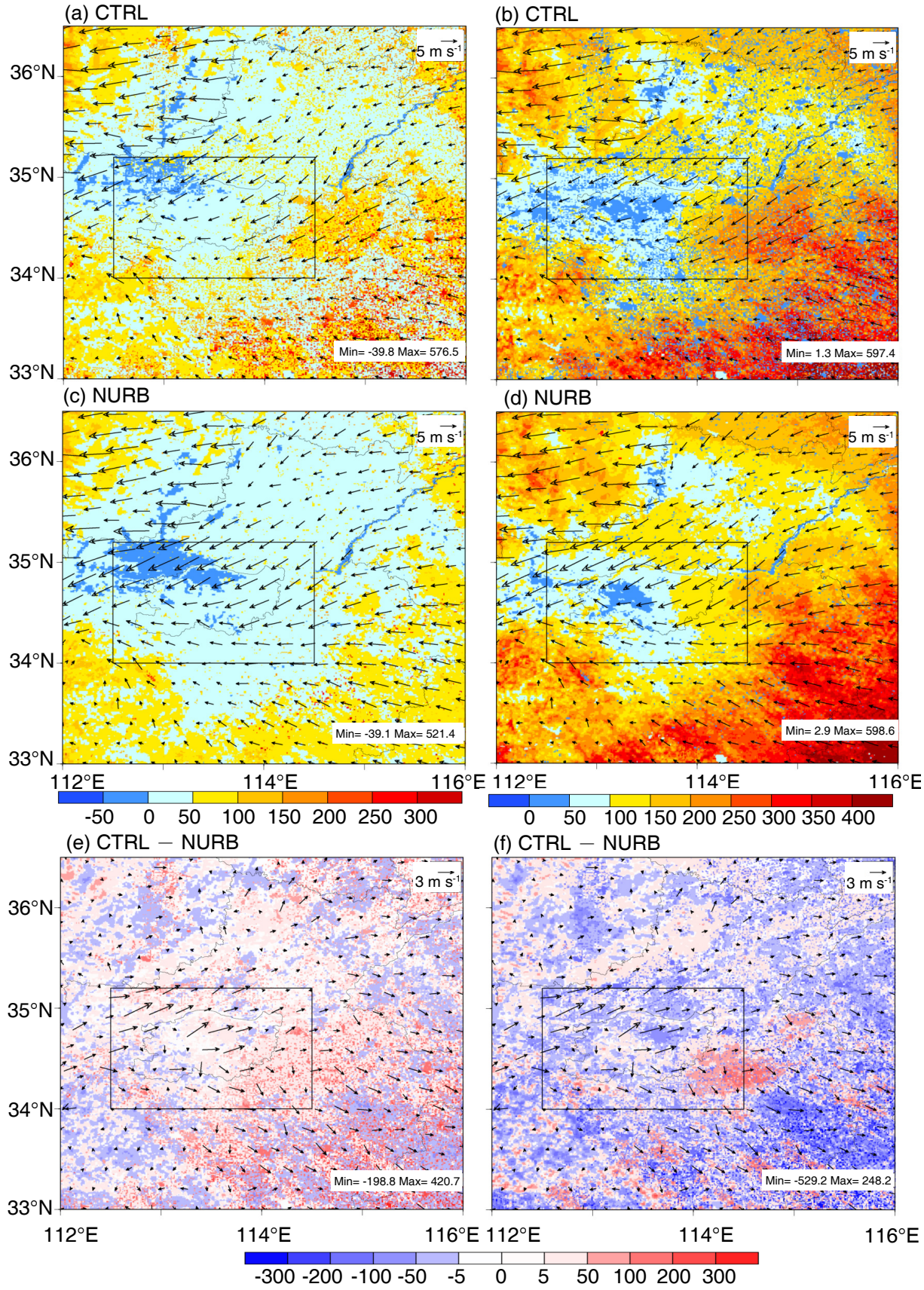

Fig. 9. Surface sensible heat flux (shadings; W m^{-2}) and surface 10-m winds (arrows) in (a) CTRL and (c) NURB, and (e) their difference (CTRL – NURB) at 1400 LST. (b), (d), (f) The same as (a), (c), (e), respectively, except for surface latent heat flux. Note different color bars are used for better illustration.

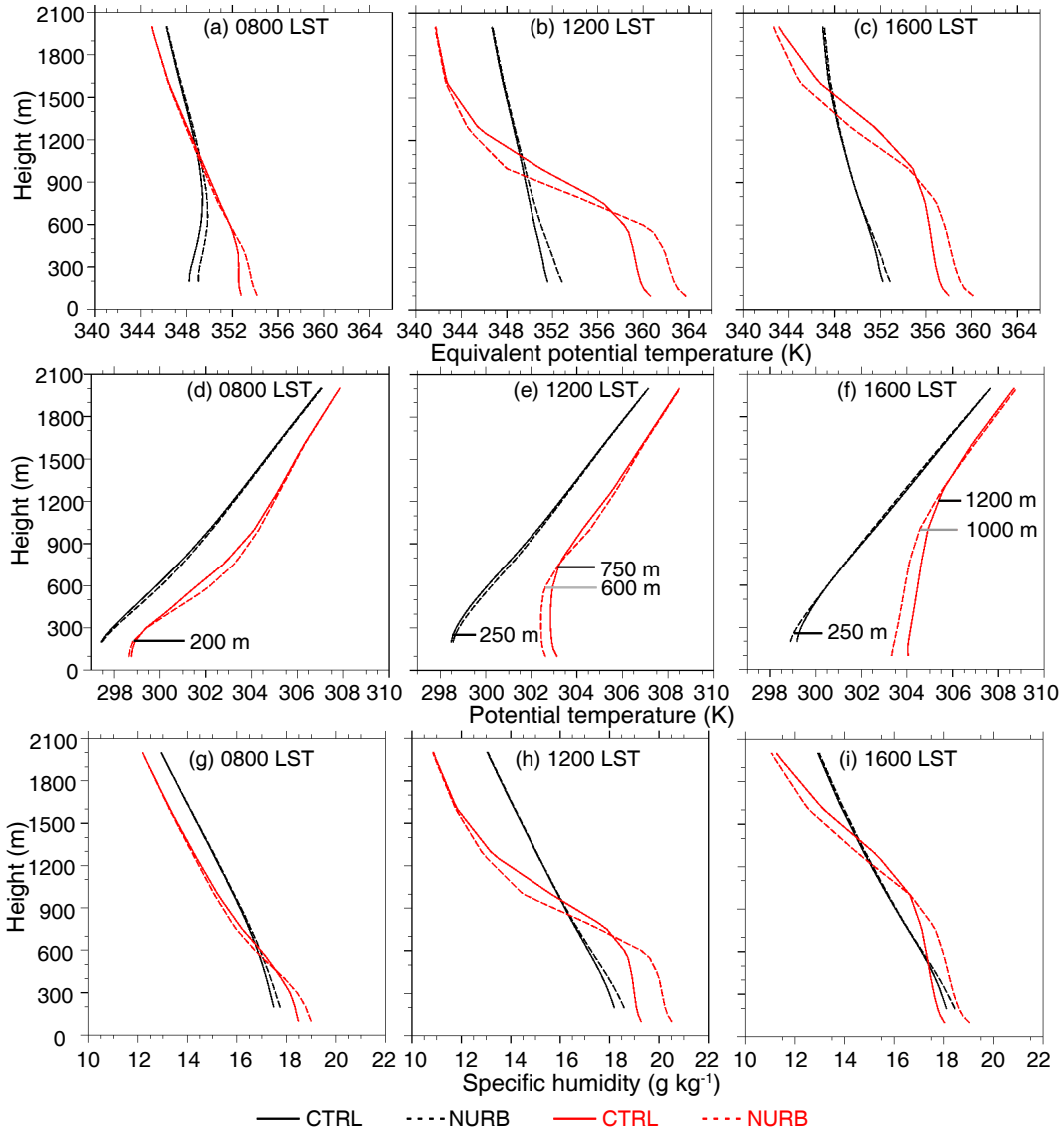

Fig. 10. Vertical profiles of (a–c) equivalent potential temperature (θ_e; units: K), (d–f) potential temperature (units: K), and (g–i) specific humidity (units: g kg^{-1}) in the ensemble mean of CTRL (solid) and NURB (dashed) at three selected times. The black and red lines denote values averaged over the key region and the region to its southeast, as shown in Figs. 2b and c, respectively. In (d)–(f), the PBL tops are labeled.

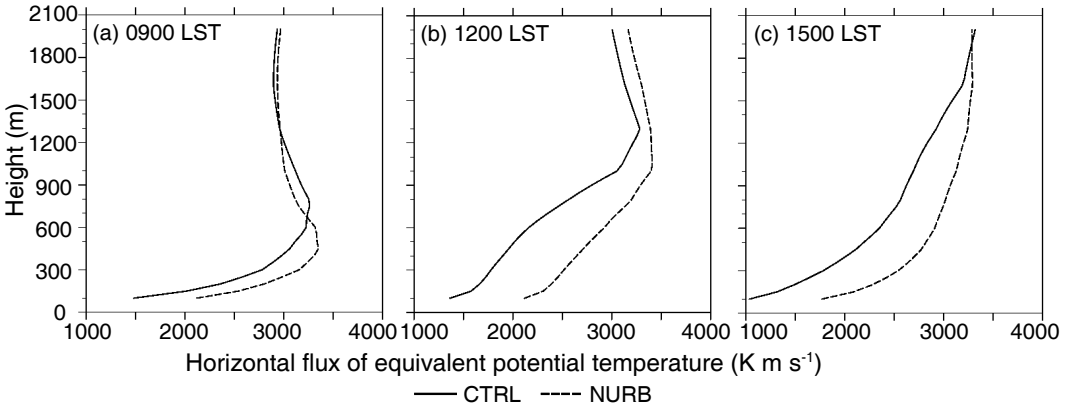

Fig. 11. Horizontal flux of θ_e (K m s^{-1}) across line CD in the ensemble mean of CTRL (solid) and NURB (dashed). Positive values denote northwestward flux, i.e., toward the key region. The location of line CD is shown in Figs. 2b and c.

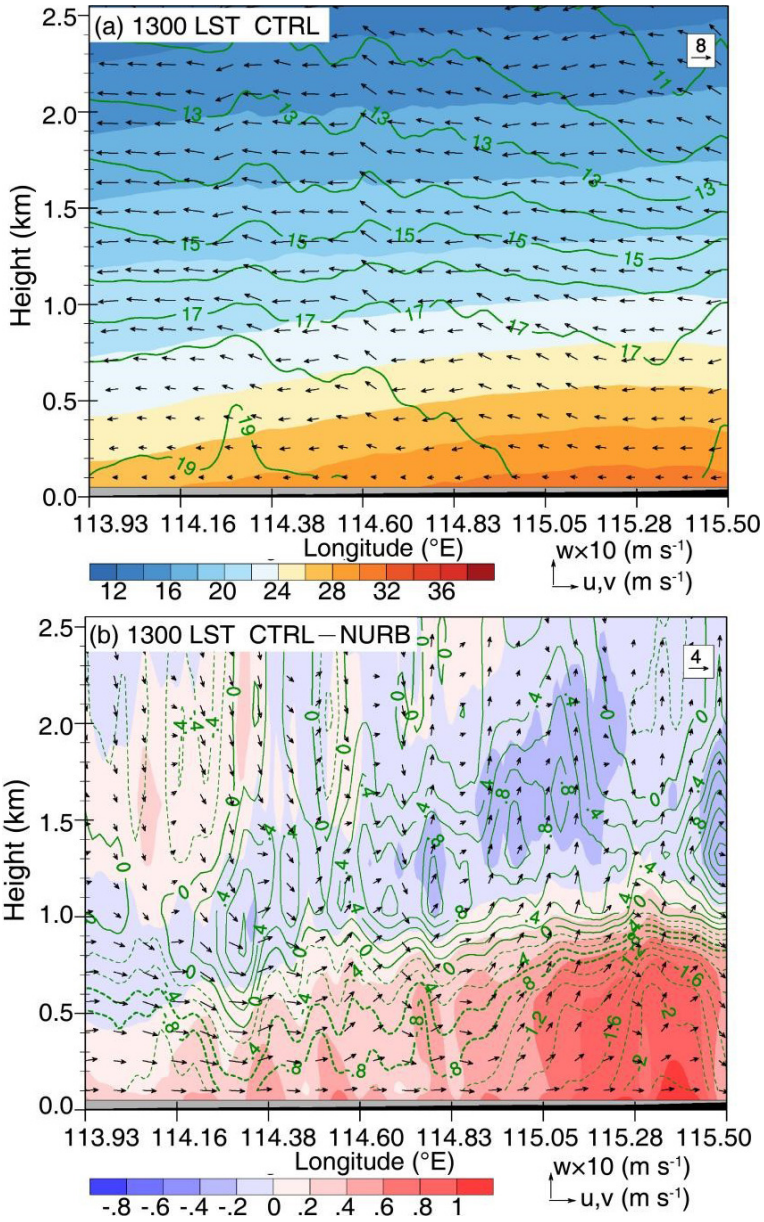

Fig. 12. (a) Temperature (shadings; °C), specific humidity (green lines; g kg^{-1}), in-plane wind vectors (vertical velocity multiplied by 10), and (b) their differences between CTRL and NURB (CTRL minus NURB) along line AB (location shown in Figs. 2b and c) at 1300 LST. In (b), solid and dashed green lines denote positive and negative values, respectively. Results shown are the ensemble means.

(NURB). A careful verification of the CTRL results is made, followed by analyses of the urban influences on the rainfall over Zhengzhou and the relevant physical processes, mainly through comparing the two ensembles. Major conclusions are as follows.

1) The CTRL experiment reasonably reproduces the spatiotemporal evolution of rainstorms and the 24-h rainfall accumulation over the key region of extreme rainfall, although the maximum hourly rainfall is underestimated and displaced to the west or southwest by most members.

2) The ensemble mean hourly rainfall accumulation over the key region is reduced throughout the day, by about 5% during the earlier nocturnal hours gradually increasing to about 30% in the late evening hours. The 24-h rainfall accumulation over the key region is reduced by 13% in the ensemble mean, and the maximum hourly rainfall over Zhengzhou is reduced by 15–70 mm in individual members of CTRL relative to NURB.

3) The urban-induced reduction in the simulated rainfall is closely associated with numerous cities/towns to the south, southeast, and east of Zhengzhou. Their heating effects jointly lead to the formation of anomalous upward

motion in and above the PBL, which not only exaggerates the PBL drying effect due to reduced evapotranspiration but also enhances the wind stilling effect due to increased surface roughness in urban areas. As a result, the lateral inflows of moisture and higher θ_e to Zhengzhou from the south and east decrease, and the area of convective updrafts (>2 m s^{-1}) over the key region is reduced.

4) The influence of Zhengzhou city on the July 20 case seems to be limited, as the persistent rainfall over Zhengzhou during 18 to 20 July 2021 significantly weakens its UHI effect.

This study demonstrates that the extensively distributed, upstream urban areas could jointly make non-negligible impacts on transportation of moisture and higher-θ_e air in

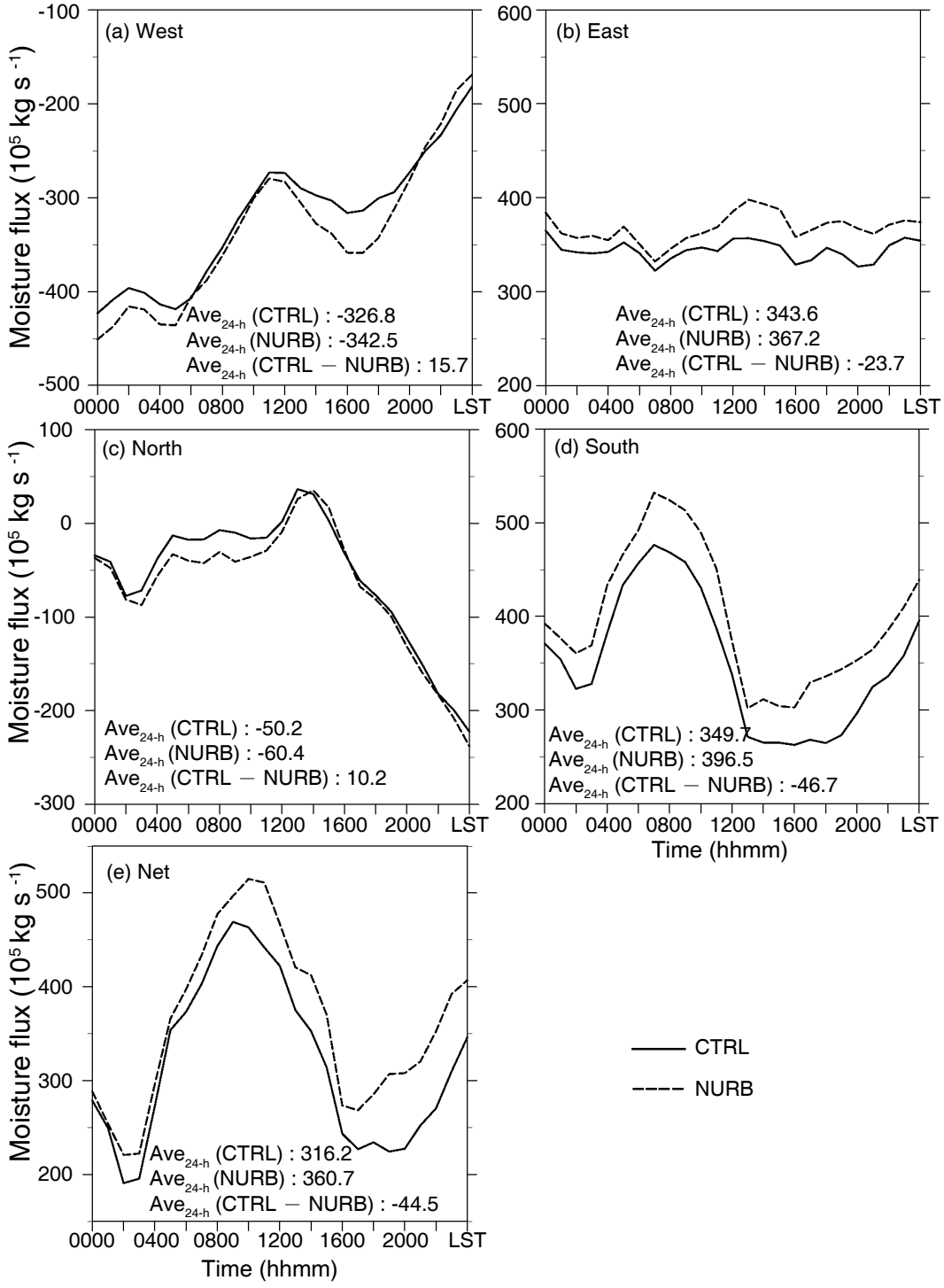

Fig. 13. Vertically integrated water vapor flux (from ground to 800 hPa) across the four boundaries of the key region (positive inward and negative outward) in the ensemble mean of CTRL (solid) and NURB (dashed). Their 24-h averages and differences (CTRL minus NURB) are labeled.

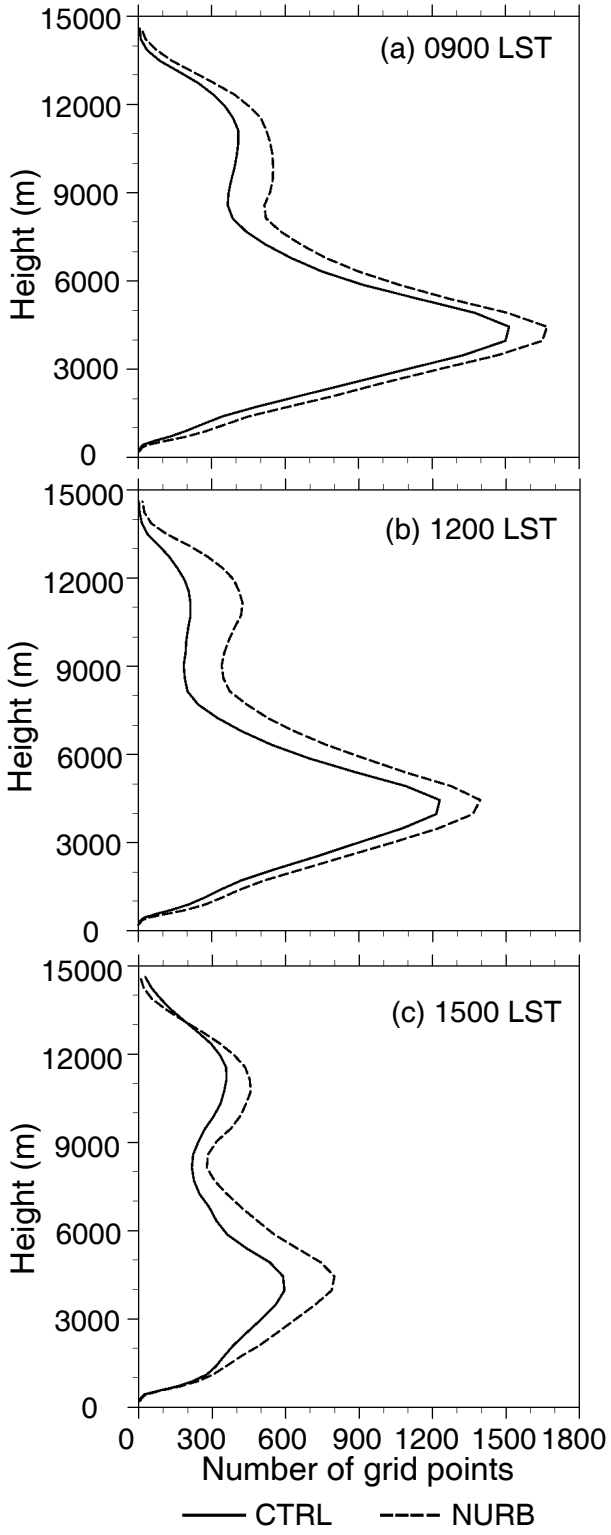

Fig. 14. Vertical profiles of number of grid points with $w >$ 2 m s^{-1} over the key region averaged among the 11 members of CTRL (solid) and NURB (dashed), respectively. There are a total of 26 055 grid points inside the key region in d3.

the PBL, leading to rainfall reduction to some extent over the downstream city where the local UHI effect is significantly reduced by rainfall. This mechanism has been paid little attention by previous studies on the relationship between heavy rainfall and urbanization, which have mainly emphasized urbanization-induced modifications to thermodynamic structure and local flow patterns in the PBL during the preconvective period. However, we should acknowledge one major weakness associated with the WRF simulations, namely, the model underestimates the historical hourly rain rate (201.9 mm), and a majority of members displace it westward or southwestward, i.e., to the urban–rural fringe areas where the surface is less impervious and relatively less residents are living. Considering this weakness and the randomness of the occurrence of such extreme hourly rainfall, the results from this study do not necessarily mean that the historical hourly rain rate over the central downtown of Zhengzhou city on 20 July 2021 would be even more extreme without the urbanization. Moreover, whether the increased roughness of Zhengzhou city contributes to production of the historical hourly rain rate by possibly enhancing the surface convergence is still unclear. Furthermore, effects of the anthropogenic aerosol emissions on the July 20 case deserve future investigation.

Acknowledgements. The National Natural Science Foundation of China (Grant Nos. 42030610 and 42075083) and the Innovation and Development Project of China Meteorological Administration (CXFZ2022J014) supported this study. We thank Prof. Xiuqun YANG (Nanjing University) for very helpful discussions. We are grateful to National Meteorological Information Center of the China Meteorological Administration for providing the observational surface datasets (http://data.cma.cn/en/?r=data/detail&dataCode=A.0012.0001). The ERA5 data were downloaded from https://cds.climate.copernicus.eu/cdsapp#!/dataset/reanalysis-era5-pressure-levels?tab=form.

REFERENCES

Abulikemu, A., Y. Wang, R. X. Gao, Y. Wang, and X. Xu, 2019: A numerical study of convection initiation associated with a gust front in Bohai Bay region, North China. *J. Geophys. Res. Atmos.*, **124**, 13 843–13 860, https://doi.org/10.1029/2019JD030883.

Bell, T. L., D. Rosenfeld, and K.-M. Kim, 2009: Weekly cycle of lightning: Evidence of storm invigoration by pollution. *Geophys. Res. Lett.*, **36**, L23805, https://doi.org/10.1029/2009GL040915.

Bornstein, R. D., and Q. L. Lin, 2000: Urban heat islands and summertime convective thunderstorms in Atlanta: Three case studies. *Atmos. Environ.*, **34**, 507–516, https://doi.org/10.1016/S1352-2310(99)00374-X.

Bougeault, P., and P. Lacarrere, 1989: Parameterization of orography-induced turbulence in a mesobeta-scale model. *Mon. Wea. Rev.*, **117**, 1872–1890, https://doi.org/10.1175/1520-0493(1989)117<1872:POOITI>2.0.CO;2.

Changnon, S. A. Jr., 1969: Recent studies of urban effects on precipitation in the United States. *Bull. Amer. Meteor. Soc.*, **50**, 411–421, https://doi.org/10.1175/1520-0477-50.6.411.

Changnon, S. A. Jr., R. G. Semonin, A. H. Auer, R. R. Braham Jr., and J. M. Hales, 1981: *METROMEX: A Review and Summary*. *Meteor. Monogr.,* No. 40, Amer. Meteor. Soc., 81 pp.

Chen, F., and J. Dudhia, 2001: Coupling an advanced land surface –hydrology model with the Penn State–NCAR MM5 modeling system. Part I: Model implementation and sensitivity. *Mon. Wea. Rev.*, **129**, 569–585, https://doi.org/10.1175/1520-0493(2001)129<0569:CAALSH>2.0.CO;2.

Craig, K., and R. Bornstein, 2002: MM5 simulations of urban induced convective precipitation over Atlanta. Preprints, *Fourth Symposium on the Urban Environment*, Norfolk, VA, Amer. Meteor. Soc., 1.3. [Available online from https://ams.confex.com/ams/AFMAPUE/techprogram/paper_38803.html]

Davis, C. A., and T. J. Galarneau Jr., 2009: The vertical structure of mesoscale convective vortices. *J. Atmos Sci.*, **66**, 686–704, https://doi.org/10.1175/2008JAS2819.1.

Doan, Q.-V., A. Dipankar, A. Simón-Moral, C. Sanchez, V. Prasanna, M. Roth, and X.-Y. Huang, 2021: Urban-induced modifications to the diurnal cycle of rainfall over a tropical city. *Quart. J. Roy. Meteor. Soc.*, **147**, 1189–1201, https://doi.org/10.1002/qj.3966.

Dudhia, J., 1989: Numerical study of convection observed during the winter monsoon experiment using a mesoscale two ‐ dimensional model. *J. Atmos. Sci.*, **46**, 3077–3107, https://doi.org/10.1175/1520-0469(1989)046<3077:NSOCOD>2.0.CO;2.

ECMWF, 2017: ERA5 reanalysis. Research data archive at the National Center for Atmospheric Research, Computational and Information System Laboratory, https://doi.org/10.5065/D6X34W69.

Ek, M. B., K. E. Mitchell, Y. Lin, E. Rogers, P. Grunmann, V. Koren, G. Gayno, and J. D. Tarpley, 2003: Implementation of Noah land surface model advances in the National Centers for Environmental Prediction operational mesoscale Eta Model. *J. Geophys. Res. Atmos.*, **108**, 8851, https://doi.org/10.1029/2002JD003296.

Fu, X. S., X.-Q. Yang, and X. G. Sun, 2019: Spatial and diurnal variations of summer hourly rainfall over three super city clusters in eastern China and their possible link to the urbanization. *J. Geophys. Res. Atmos.*, **124**, 5445–5462, https://doi.org/10.1029/2019JD030474.

Guo, X. L., D. H. Fu, and J. Wang, 2006: Mesoscale convective precipitation system modified by urbanization in Beijing city. *Atmospheric Research*, **82**, 112–126, https://doi.org/10.1016/j.atmosres.2005.12.007.

Hjelmfelt, M. R., 1982: Numerical simulation of the effects of St. Louis on mesoscale boundary-layer airflow and vertical air motion: Simulations of urban vs non-urban effects. *J. Appl. Meteorol.*, **21**, 1239–1257, https://doi.org/10.1175/1520-0450(1982)021<1239:NSOTEO>2.0.CO;2.

Huff, F. A., and J. L. Vogel, 1978: Urban, topographic and diurnal effects on rainfall in the St. Louis region. *J. Appl. Meteorol.*, **17**, 565–577, https://doi.org/10.1175/1520-0450(1978)017<0565:UTADEO>2.0.CO;2.

Janjić, Z. I., 1990: The step-mountain coordinate: Physical package. *Mon. Wea. Rev.*, **118**(7), 1429–1443, https://doi.org/10.1175/1520-0493(1990)118<1429:TSMCPP>2.0.CO;2.

Janjić, Z. I., 2002: Nonsingular implementation of the Mellor–Yamada level 2.5 scheme in the NCEP Meso model. NCEP Office Note 437, 61 pp.

Jiang, X. L., Y. L. Luo, D.-L. Zhang, and M. W. Wu, 2020: Urbanization enhanced summertime extreme hourly precipitation over the Yangtze River Delta. *J. Climate*, **33**, 5809–5826, https://doi.org/10.1175/JCLI-D-19-0884.1.

Jin, M. L., and J. M. Shepherd, 2008: Aerosol relationships to warm season clouds and rainfall at monthly scales over East China: Urban land versus ocean. *J. Geophys. Res. Atmos.*, **113**, D24S90, https://doi.org/10.1029/2008JD010276.

Kain, J. S., 2004: The Kain-Fritsch convective parameterization: An update. *J. Appl. Meteorol.*, **43**(1), 170–181, https://doi.org/10.1175/1520-0450(2004)043<0170:TKCPAU>2.0.CO;2.

Kishtawal, C. M., D. Niyogi, M. Tewari, R. A. Pielke, and J. M. Shepherd, 2010: Urbanization signature in the observed heavy rainfall climatology over India. *International Journal of Climatology*, **30**, 1908–1916, https://doi.org/10.1002/joc.2044.

Li, H. Q., X. P. Cui, and D.-L. Zhang, 2017: Sensitivity of the initiation of an isolated thunderstorm over the Beijing metropolitan region to urbanization, terrain morphology and cold outflows. *Quart. J. Roy. Meteor. Soc.*, **143**, 3153–3164, https://doi.org/10.1002/qj.3169.

Li, Y., and Coauthors, 2020: Strong intensification of hourly rainfall extremes by urbanization. *Geophys. Res. Lett.*, **47**, e2020GL088758, https://doi.org/10.1029/2020GL088758.

Liang, P., and Y. H. Ding, 2017: The long-term variation of extreme heavy precipitation and its link to urbanization effects in Shanghai during 1916–2014. *Adv. Atmos. Sci.*, **34**, 321–334, https://doi.org/10.1007/s00376-016-6120-0.

Lim, K.-S. S., and S.-Y. Hong, 2010: Development of an effective double-moment cloud microphysics scheme with prognostic cloud condensation nuclei (CCN) for weather and climate models. *Mon. Wea. Rev.*, **138**, 1587–1612, https://doi.org/10.1175/2009MWR2968.1.

Martilli, A., 2002: Numerical study of urban impact on boundary layer structure: Sensitivity to wind speed, urban morphology, and rural soil moisture. *J. Appl. Meteorol.*, **41**, 1247–1266, https://doi.org/10.1175/1520-0450(2002)041<1247:NSOUIO>2.0.CO;2.

Matheson, M. A., and Y. Ashie, 2008: The effect of changes of urban surfaces on rainfall phenomenon as determined by a non-hydrostatic mesoscale model. *J. Meteor. Soc. Japan*, **86**, 733–751, https://doi.org/10.2151/jmsj.86.733.

Miao, S. G., F. Chen, Q. C. Li, and S. Y. Fan, 2011: Impacts of urban processes and urbanization on summer precipitation: A case study of heavy rainfall in Beijing on 1 August 2006. *J. Appl. Meteorol. Climatol.*, **50**, 806–825, https://doi.org/10.1175/2010JAMC2513.1.

Mlawer, E. J., S. J. Taubman, P. D. Brown, M. J. Iacono, and S. A. Clough, 1997: Radiative transfer for inhomogeneous atmosphere: RRTM, a validated correlated ‐ k model for the longwave. *J. Geophys. Res. Atmos.*, **102**(D14), 16,663–16,682,

https://doi.org/10.1029/97JD00237.

Morrison, H., and J. A. Milbrandt, 2015: Parameterization of cloud microphysics based on the prediction of bulk ice particle properties. Part I: Scheme description and idealized tests. *J. Atmos. Sci.*, **72**, 287–311, https://doi.org/10.1175/JAS-D-14-0065.1.

Morrison, H., G. Thompson, and V. Tatarskii, 2009: Impact of cloud microphysics on the development of trailing stratiform precipitation in a simulated squall line: Comparison of one- and two-moment schemes. *Mon. Wea. Rev.*, **137**(3), 991–1007, https://doi.org/10.1175/2008MWR2556.1.

Niyogi, D., P. Pyle, M. Lei, S. P. Arya, C. M. Kishtawal, M. Shepherd, F. Chen, and B. Wolfe, 2011: Urban modification of thunderstorms: An observational storm climatology and model case study for the Indianapolis urban region. *J. Appl. Meteorol. Climatol.*, **50**, 1129–1144, https://doi.org/10.1175/2010JAMC1836.1.

Ntelekos, A. A., J. A. Smith, L. Donner, J. D. Fast, W. I. Gustafson Jr., E. G. Chapman, and W. F. Krajewski, 2009: The effects of aerosols on intense convective precipitation in the northeastern United States. *Quart. J. Roy. Meteor. Soc.*, **135**, 1367–1391, https://doi.org/10.1002/qj.476.

Rosenfeld, D., 2000: Suppression of rain and snow by urban and industrial air pollution. *Science*, **287**, 1793–1796, https://doi.org/10.1126/science.287.5459.1793.

Skamarock, W. C., and Coauthors, 2008: A description of the Advanced Research WRF version 3. NCAR Tech. Note NCAR/TN-4751STR, 113 pp.

Sun, X. Y., Y. L. Luo, X. Y. Gao, M. W. Wu, M. X. Li, L. Huang, D. L. Zhang, and H. M. Xu, 2021: On the localized extreme rainfall over the Great Bay area in South China with complex topography and strong UHI effects. *Mon. Wea. Rev.*, **149**, 2777–2801, https://doi.org/10.1175/MWR-D-21-0004.1.

Taylor, K. E., 2001: Summarizing multiple aspects of model performance in a single diagram. *J. Geophys. Res. Atmos.*, **106**, 7183–7192, https://doi.org/10.1029/2000JD900719.

Thompson, G., and T. Eidhammer, 2014: A study of aerosol impacts on clouds and precipitation development in a large winter cyclone. *J. Atmos. Sci.*, **71**(10), 3636–3658, https://doi.org/10.1175/JAS-D-13-0305.1.

Thompson, G., P. R. Field, R. M. Rasmussen, and W. D. Hall, 2008: Explicit forecasts of winter precipitation using an improved bulk microphysics scheme. Part II: Implementation of a new snow parameterization. *Mon. Wea. Rev.*, **136**, 5095–5115, https://doi.org/10.1175/2008MWR2387.1.

Wai, K. M., and Coauthors, 2017: Observational evidence of a long-term increase in precipitation due to urbanization effects and its implications for sustainable urban living. *Science of The Total Environment*, **599–600**, 647–654, https://doi.org/10.1016/j.scitotenv.2017.05.014.

Wang, X. M., F. Chen, Z. Y. Wu, M. G. Zhang, M. Tewari, A. Guenther, and C. Wiedinmyer, 2009: Impacts of weather conditions modified by urban expansion on surface ozone: Comparison between the Pearl River Delta and Yangtze River Delta regions. *Adv. Atmos. Sci.*, **26**, 962–972, https://doi.org/10.1007/s00376-009-8001-2.

Wei, P., and Coauthors, 2022: On key dynamical processes supporting the 21.7 Zhengzhou record-breaking hourly rainfall in China. *Adv. Atmos. Sci.*, https://doi.org/10.1007/s00376-022-2061-y.

Wu, M. W., Y. L. Luo, F. Chen, and W. K. Wong, 2019: Observed link of extreme hourly precipitation changes to urbanization over coastal South China. *J. Appl. Meteorol. Climatol.*, **58**, 1799–1819, https://doi.org/10.1175/JAMC-D-18-0284.1.

Xiao, C., P. L. Wu, L. X. Zhang, and L. C. Song, 2016: Robust increase in extreme summer rainfall intensity during the past four decades observed in China. *Scientific Reports*, **6**, 38506, https://doi.org/10.1038/srep38506.

Xu, X., M. Xue, Y. Wang, 2015: Mesovortices within the 8 May 2009 Bow Echo over the Central United States: Analyses of the characteristics and evolution based on Doppler radar observations and a high-resolution model simulation. *Mon. Wea. Rev.*, **143**, 2266–2290, https://doi.org/10.1175/MWR-D-14-00234.1.

Yang, L., J. Smith, and D. Niyogi, 2019: Urban impacts on extreme monsoon rainfall and flooding in complex terrain. *Geophys. Res. Lett.*, **46**, 5918–5927, https://doi.org/10.1029/2019GL083363.

Yang, L., J. A. Smith, M. L. Baeck, E. Bou-Zeid, S. M. Jessup, F. Q. Tian, and H. P. Hu, 2014: Impact of urbanization on heavy convective precipitation under strong large-scale forcing: A case study over the Milwaukee-Lake Michigan region. *Journal of Hydrometeorology*, **15**, 261–278, https://doi.org/10.1175/JHM-D-13-020.1.

Yin, J. F., D.-L. Zhang, Y. L. Luo, and R. Y. Ma, 2020: On the extreme rainfall event of 7 May 2017 over the coastal city of Guangzhou. Part I: impacts of urbanization and orography. *Mon. Wea. Rev.*, **148**, 955–979, https://doi.org/10.1175/MWR-D-19-0212.1.

Yin, J. F., H. D. Gu, X. D. Liang, M. Yu, J. S. Sun, Y. X. Xie, F. Li, and C. Wu, 2022: A possible dynamic mechanism for rapid production of the extreme hourly rainfall in Zhengzhou city on 20 July 2021. *J. Meteor. Res.*, **36**, 6–25, https://doi.org/10.1007/s13351-022-1166-7.

Zhang, C. L., F. Chen, S. G. Miao, Q. C. Li, X. A. Xia, and C. Y. Xuan, 2009a: Impacts of urban expansion and future green planting on summer precipitation in the Beijing metropolitan area. *J. Geophys. Res. Atmos.*, **114**, D02116, https://doi.org/10.1029/2008JD010328.

Zhang, D.-L., 2020: Rapid urbanization and more extreme rainfall events. *Science Bulletin*, **65**, 516–518, https://doi.org/10.1016/j.scib.2020.02.002.

Zhang, Q., C.-Y. Xu, S. Becker, Z. X. Zhang, Y. D. Chen, and M. Coulibaly, 2009b: Trends and abrupt changes of precipitation maxima in the Pearl River basin, China. *Atmospheric Science Letters*, **10**, 132–144, https://doi.org/10.1002/asl.221.

Zhong, S., and X.-Q. Yang, 2015: Ensemble simulations of the urban effect on a summer rainfall event in the great Beijing metropolitan area. *Atmospheric Research*, **153**, 318–334, https://doi.org/10.1016/j.atmosres.2014.09.005.

Zhong, S., Y. Qian, C. Zhao, R. Leung, and X. Q. Yang, 2015: A case study of urbanization impact on summer precipitation in the greater Beijing metropolitan area: Urban heat island versus aerosol effects. *J. Geophys. Res. Atmos.*, **120**, 10 903–10 914, https://doi.org/10.1002/2015JD023753.